RSC Advances

ROYAL SOCIETY OF CHEMISTRY

www.rsc.org/advances

RSC Advances RSCPublishing

ARTICLE

Synergy between vanadium and molybdenum in bimetallic ZSM-5 supported catalysts for ethylene ammoxidation

Cite this: DOI: 10.1039/x0xx00000x

Received ooth January 2016,
Accepted ooth January 2016

DOI: 10.1039/x0xx00000x

www.rsc.org/

Baker Rhimi,*[a] Mourad Mhamdi,[ab] Venkata Narayana Kalevaru,[c] Andreas Martin.[c]

Ammoxidation of ethylene to acetonitrile was studied on V/ZSM-5, Mo/ZSM-5 and V-Mo/ZSM-5 catalysts prepared by solid-state ion exchange method. The physico-chemical properties were investigated by means of XRD, N_2 physisorption, ^{27}Al and ^{29}Si MAS NMR, UV–Vis DRS, XPS, pyridine-IR and FT-IR spectroscopies and H_2-TPR/O_2-TPO. Based on characterization results, M-O_x (M = V or Mo) species react with zeolite protons during the exchange process and generate new Lewis acid sites, which act as redox centers. The M-O_x species are essentially, monomeric and dimeric/polymeric species or metal oxide crystallites (less than 4 nm) highly dispersed in the channel and/or on the external surface of zeolite. For Mo/ZSM-5 sample, the formation of $Al_2(MoO_4)_3$ nano-crystallites was observed. UV–Vis DRS and TPR results showed that V and Mo species in all catalysts are mainly in the highest oxidation states. The V-Mo/ZSM-5 catalyst exhibited a more reversible behavior of the M-O_x centers throughout the H_2/O_2 redox cycles than those in V/ZSM-5 and Mo/ZSM-5 catalysts. The best catalytic performance was achieved over the bimetallic V-Mo/ZSM-5 catalyst. These results revealed that the partial substitution of molybdenum with vanadium has a positive effect on the activity and the selectivity to acetonitrile. This implies clearly that a synergetic effect between V and Mo species plays an important role in the ammoxidation reaction. This synergetic effect is related to the existence of electronic interaction at short range order between the V and Mo species, which may influence the catalyst redox properties.

1 Introduction

There is nowadays a great deal of research interest for the partial oxidation reactions of light hydrocarbons into more valuable compounds. One of these reactions is the ethylene ammoxidation that refers to the formation of acetonitrile (ACN) by partial oxidation of ethylene in the presence of ammonia. ACN is an important base chemical product with a variety of industrial applications.[1] For the direct ammoxidation (Eq. (1)), several catalyst systems have been studied, e.g., mixed oxides such as Cr-Nb-Mo-O catalyst[2] and zeolite-supported transition metals catalysts.[3-5] Up to now, most research work has focused on zeolite-supported transition metals catalysts prepared by ion exchange method which can be carried out either in liquid solution or by solid-state exchange reaction. The solid-state ion exchange reaction between a zeolite and a solid precursor salt has received considerable recent attention.[6] This method consists in heating a mixture of the zeolite and the active phase salt precursor. Over-stoichiometric exchanges can be expected by solid-state ion exchange while they cannot be obtained in solution. Furthermore, with solid-state reaction, parameters difficult to control such as pH, cation size and solvation phenomena are avoided.[7,8]

$$C_2H_4 + O_2 + NH_3 \rightarrow CH_3CN + 2\ H_2O \qquad (1)$$

Recently, Li and Armor[3], Wichterlova and co-workers[9] and Mhamdi and al.[10] claim higher activity of Co exchanged zeolite catalysts with BEA and MFI topologies in ethylene ammoxidation. Among different supported cobalt catalysts, Co/ZSM-5 systems are the most commonly used ones for the ethylene ammoxidation into acetonitrile. The unique properties of zeolite ZSM-5 in terms of surface area, porous structure and acidity could justify the high activity of Co/ZSM-5 systems.

On the other hand, molybdenum-zeolites, especially Mo/HZSM-5 systems have also been studied in recent years due to their active and selective nature for different partial oxidation reactions, for example, methane dehydroaromatization[11,12] and selective catalytic reduction of NO_x etc.[13] Numerous spectroscopic studies, aimed to highlight the nature of the surface Mo structures on/in Mo/HZSM-5 catalysts. In general, the Mo oxide species are highly dispersed on the ZSM-5 surface and are associated with the Brönsted acid sites of the ZSM-5 if the Mo loading is <8 wt% and the calcination temperature is below 550 °C. Nonetheless, MoO_3 and $Al_2(MoO_3)_4$ crystallites can be detected with increasing Mo loading and calcination temperature. Furthermore, the most active and selective catalyst systems used for different partial oxidation processes contain vanadium as key component. Among them, V–

Mo–O,[14] V–Sb–O[15] and V–Ti–O[16] based catalysts, that are either supported on various oxides or promoted by further transition metals, are extensively investigated by various research groups. These bi-component or multi-component composite catalysts are composed of one or more catalytically active sites and a functional support, in which the cooperation/interaction between the catalytic components and/or the support materials can significantly enhance both the catalytic activity and selectivity of target products. Thus, a synergetic effect does exist in the catalytic systems and may play an important or decisive role, in various catalytic oxidation reactions.

In the present study, NH_4-ZSM-5 zeolite was used as the support. Then the catalysts containing vanadium alone, molybdenum alone and vanadium-molybdenum together were prepared by solid-state ion-exchange method. These catalysts were characterized by several characterization techniques. The objective of this work was to study the effect of vanadium on the properties of molybdenum based catalyst supported on ZSM-5 support. We report for the first time, how on zeolite a synergetic effect between vanadium and molybdenum can improve the catalytic performance in ethylene ammoxidation into acetonitrile.

[a] Université de Tunis El Manar, Faculté des Sciences de Tunis, Laboratoire de Chimie des Matériaux et Catalyse, 2092, Tunis, Tunisie.

[b] Université de Tunis El Manar, Institut Supérieur des Technologies Médicales de Tunis, 9 Avenue du Docteur Zouhaier Essafi, 1006, Tunis, Tunisie.

[c] Leibniz-Institut für Katalyse e. V. an der Universität Rostock, Albert-Einstein-Str. 29a, D-18059 Rostock, Germany.

* Corresponding author. E-mail: rhimi.baker@gmail.com

2 Experimental

2.1 Catalyst preparation

NH_4-form of ZSM-5 (Si/Al = 26) supplied by Zeolyst International Inc. was used as starting material. V-Mo/ZSM-5 catalyst was prepared by solid-state ion exchange in two steps. First, 1g of zeolite and ammonium metavanadate NH_4VO_3 (98%, PROLABO) in a ratio of 2 wt% were finely ground and mixed in a mortar for 15 min at ambient conditions. The resulting mixture was then heated in a helium flow (30 mL/min) up to 500°C (heating rate: 2 °C/min) and left at 500 °C overnight (12 h). Then the obtained solid was finely ground and mixed with the molybdenum acetylacetonate precursor (98%, MERCK) in the molar ratio V + Mo/Al = 1 and heated again for 12 h at 500 °C in a flow of helium. Finally the catalysts were calcined in oxygen for 1 h at 500 °C in order to convert precursor sources into oxides and also to remove the coke originating from the decomposition of the acetylacetonate ligand. V/ZSM-5 and Mo/ZSM-5 catalysts were prepared by mixing in a mortar 1g of NH_4–ZSM-5 and, NH_4VO_3 in a ratio 2 wt% or molybdenum acetylacetonate in the molar ratio Mo/Al = 1, followed by helium treatment at 500 °C for 12 h (30 cm^3/min, heating rate 2 °C/min).

2.2. Catalyst characterization

BET surface areas and pore volumes of the samples were determined with a Micromeritics ASAP-2020 analyzer with N_2 as the adsorbate at −196 °C.

Phase analysis of all solids was carried out using X-ray diffraction (XRD, STADIP, Stoe) using Cu Kα1 radiation (1.5406 Å). The 2θ range was varied between 2 and 80°, with a step size of 0.02°. The chemical element (Mo, V, Si, Al) content of catalysts was determined by ICP (Optima 3000XL, Perkin-Elmer). All the samples were analysed twice and the results presented here are the average of two values.

UV–vis spectra of Mo and V species were recorded under ambient conditions using Perkin Elmer Lambda 45 spectrophotometer equipped with a diffuse reflectance attachment with an integrating sphere coated with $BaSO_4$. Diffuse reflectance spectra were analyzed by Kubelka–Munk treatments.

FTIR spectra were recorded on a Perkin Elmer (Spectrum BX) spectrometer in the wavenumber range 4000–400 cm^{-1} using the KBr disc technique. Spectra were recorded in air using a 4 cm^{-1} resolution.

The Pyridine-IR experiments were carried out with a Bruker IFS 66 spectrometer (2 cm^{-1} resolution, 100 scans) equipped with a heatable and evacuable IR cell with CaF_2 windows, which is connected to a gas dosing/evacuation system. For these experiments, the powder samples were pressed into self-supporting discs (50 mg, Ø 20 mm). All the IR spectra were measured after activation of samples at 400 °C with air flow for 30 min. For the adsorption of pyridine, the samples were first evacuated then connected with pyridine vapour at room temperature. Finally, desorption was performed under vacuum treatment at 200 °C.

The XPS data were recorded with a VG ESCALAB 220iXL unit using Mg Kα radiation (E = 1253.6 eV) at a base pressure of the UHV chamber. Spectra were analyzed with CasaXPS software and RSF database by fitting after Shirley background correction.

The ^{27}Al and ^{29}Si MAS NMR measurements were performed with a Bruker MSL 400 spectrometer at resonance frequencies of 104.26 and 79.49 MHz, respectively, and sample spinning rates of 10 kHz for ^{27}Al and 4 kHz for ^{29}Si NMR spectroscopy. Short π/12 radio frequency (rf) pulses were employed for $^{27}A1$ spectra and π/4 (rf) pulses were used for ^{29}Si spectra.

TPR and TPO (temperature-programmed oxidation) experiments were done using a Micromeritics Autochem II 2920 instrument. The catalyst powder was introduced into a quartz reactor over a porous septum (ca. 8 mm i.d.). Redox cycles (^{1st}TPR/TPO/^{2nd}TPR) were realized by carrying out three analyses in sequence: a first reduction on the oxidized sample (^{1st}TPR), an oxidation (TPO), and a second reduction (^{2nd}TPR). The sample was pre-oxidized in 5% O_2/He (20 mL/min) for 30 min at 650 °C and then cooled down to 50 °C. The ^{1st}TPR run was carried out from 50 to 900 °C in a gas consists of 5% H_2/Ar flow (20 mL/min) with a constant heating rate of 10 °C/min. The TPO analysis was carried out on the reduced samples cooled down to 50 °C using a 5% O_2/He flow (20 mL/min) from 50 to 900 °C. The oxidized sample was further reduced during the ^{2nd}TPR run, under the same experimental conditions described above. Optimum sample weights (0.08-0.13 g) corresponding to a reduction in gas flow rate of 20 mL/min had been estimated according to the equation proposed by Monti and Baiker.[17] The hydrogen consumption peaks were recorded with temperature and quantitative analysis of the TPR data, based on the peak areas, was calculated.

Ethylene ammoxidation runs were performed in a fixed bed through flow microreactor. In a typical experiment, 0.05 g of powder sample used for ethylene test and O_2 (Air Liquide 99.995%), NH_3 (Air Liquide 99.96%), C_2H_4 (Air Liquide 99.995%) and He (Air

Liquide 99.998%) supplied were commercially available gases from compressed gas cylinders. The reaction was carried out in the range of 425–500 °C and the catalysts were pretreated in helium at 500 °C for 1 h before each reaction run. A steady-state conditions for each temperature were reached within 1 h. The inlet reactant composition was 10% O_2, 10% C_2H_4 and 10% NH_3. The total flow rate was 100 mL/min by balancing with helium flow rate. Product gases were analyzed on-line by two chromatographic units, one operated with a flame ionization detector FID for analysis of organic compounds, while the other was equipped with a thermal conductivity detector TCD for analysis of inorganic compounds. The conversion and selectivity are calculated using the equations shown below:

Conversion, $$X = \frac{\sum_i y_i n_i}{y_E n_E + \sum_i y_i n_i}$$

Selectivity of reaction product (carbon basis), $$S_i = \frac{y_i n_i}{\sum_i y_i n_i}$$

Yield of product P_i (carbon basis), $Y_i = X \cdot S_i$, where y_i and y_E are the mole fractions of product and ethylene respectively; n_i and n_E are the number of carbon atoms in each molecule of reaction product and ethylene, respectively.

3. Results and discussion

3.1 Chemical analysis

Table 1 gives the elemental analysis of parent zeolite and different solids including V, Mo, Si and Al contents and Si/Al and V+Mo/Al molar ratios. The values obtained for Si and Al fit the data provided by the zeolite manufacturers. On the other hand, the V and Mo contents analyzed in the catalysts are in good agreement with those of theoretical values. Thus, it confirms that no molybdenum or vanadium is lost during the solid-state exchange reaction by sublimation. All the metals loaded are either on the external surface of the zeolite crystals or diffused inside its channels.

3.2 XRD phase analysis

The XRD patterns of synthesized catalysts along with the parent zeolite are shown in Fig.1. The obtained diffractograms are identical to that of the parent zeolite, and no reflections are seen that can be attributed to any other crystalline phases corresponding to either VO_x or MoO_x.

These results indicate that the framework of the support was still retained during the solid state reaction. Compared with the zeolite pattern, the intensities of peaks of different catalysts decreased. As known, the low-angle XRD intensities in the pattern of zeolite are sensitive to the presence of any species inside the channels. The decrease of peak intensity of low-angle XRD patterns also implies the entrance of Molybdenum and vanadium species into the channels.

Absence of crystalline phases of molybdenum oxides or vanadium oxide in all catalysts is due to the low contents (<2 wt%) of these metal oxides., We believe that some metal species (i.e. oxides, cations ...) as small crystallites (measured less than 4 nm in diameter) might be formed but cannot be detected by XRD due to their X-ray amorphous nature. Moreover, such small crystallites might be either dispersed on the external surface of zeolite crystals, or even penetrated into the channels of zeolite during the treatment.

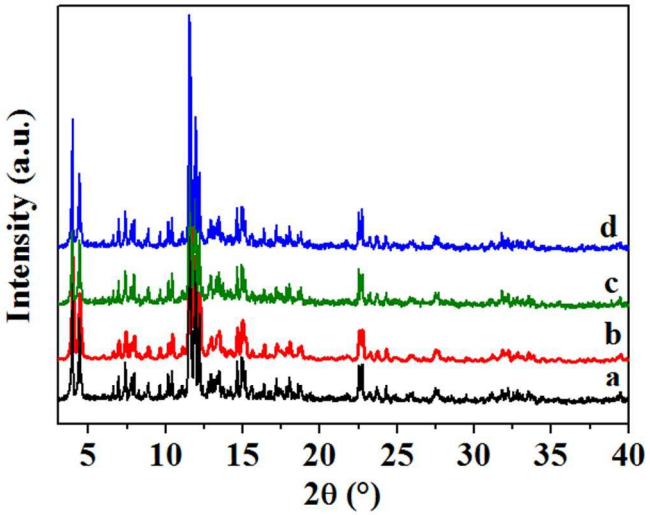

Fig.1 XRD patterns of (a) NH_4-ZSM-5, (b) V/ZSM-5, (c) Mo/ZSM-5 and (d) V-Mo/ZSM-5.

3.3 Textural properties obtained by N_2-physisorption

The textural properties obtained from the N_2-adsorption/desorption isotherms of the parent zeolite and catalysts are summarized in Table 2. Catalysts as well as the zeolite support exhibit a type I isotherm characteristic of microporous materials, although the catalysts show small hysteresis loop at higher partial pressures, which reveals some intergranular mesoporosity.

Table 1: Elemental analysis results (ICP) of catalysts.

Sample	Mo(wt.%)	V(wt.%)	Si(wt.%)	Al(wt.%)	Si/Al	V/Al	Mo/Al	V+Mo/Al
NH_4-ZSM-5	-	-	40.73	1.5	27	-		-
V/ZSM-5	-	2.03	40.92	1.4	29	0.77	-	-
Mo/ZSM-5	5.85	-	41.6	1.38	30	-	1.2	-
V-Mo/ZSM-5	2.12	1.95	40.99	1.39	29	0.77	0.43	1.2

It was reported in literature[18] that metal ions were merely deposited on the external surface of zeolites as oxide aggregates which might contribute to the calculations of textural data and such solids exhibit some degree of mesoporosity. It can be seen from Table 2 that pure NH_4-ZSM5 support exhibit the highest surface area (390 m^2/g) compared to the catalysts containing V and/or Mo. The surface areas of the catalysts are varied in the range from 361 to 386 m^2/g. It is observed that the exchange process was accompanied by a decrease of S_{BET} surface area and pore volume of the support. This effect may be attributed to the presence of oxide aggregates or aluminum-molybdates crystallites that partially block the pores inside or at the entrance of channels of the zeolite. In addition, MoO_x being heavier than that of VO_x, it has shown pronounced influence on the surface area. As a result, Mo/ZSM-5 solid exhibit relatively low surface area (358 m^2/g) compared to V/ZSM-5 solid (386 m^2/g).

Table 2 Textural properties of the investigated solids.

Sample	S_{BET} ($m^2\ g^{-1}$)	Sμ ($m^2\ g^{-1}$)	Vμ ($cm^3\ g^{-1}$)	Vp ($cm^3\ g^{-1}$)
NH_4-ZSM5	390	344	0.16	0.22
V/ ZSM-5	386	339	0.15	0.22
Mo/ ZSM-5	358	319	0.13	0.19
V-Mo/ZSM-5	361	324	0.14	0.20

S_μ= micro pore surface area; V_μ= micro pore volume

3.4 FTIR

Fig. 2 illustrates the FT-IR spectra of the parent NH_4-ZSM-5 zeolite and the solid-state reaction products in the wavenumber regions of 1400-400 cm^{-1}. The crystallinity reduction of zeolite can be evaluated by comparing the ratio of the intensity of the bands at 550 and 450 cm^{-1} with that of the parent NH_4-ZSM-5,[19,20] which was considered to be 100% crystalline. The band situated at 450 cm^{-1} corresponds to the internal vibrations of primary structural units, while the band at 550 cm^{-1} is attributed to the vibration of larger parts of the structure.[21] Considering a value of 1.62 for well crystalline ZSM-5, the observed values of 1.61, 1.58 and 1.34, respectively for V/ZSM-5, V-Mo/ZSM-5 and Mo/ZSM-5 samples clearly demonstrate that no significant damage to the zeolite host structure (after the solid state ion exchange reaction) is occurred.

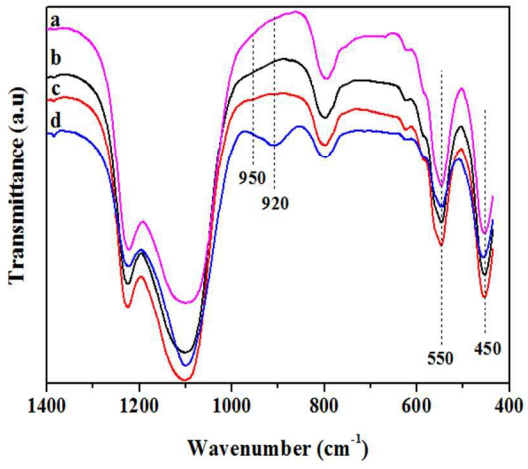

Fig.2 FT-IR spectra of (a) NH_4-ZSM-5, (b) V/ZSM-5, (c) V-Mo/ZSM-5 and (d) Mo/ZSM-5.

For Mo/ZSM-5 catalysts, a new broad band appears at around 920 cm^{-1} while for V-Mo/ZSM-5, two new bands appear in the vicinity of 900-1000 cm^{-1}. This band is assigned to the stretching vibration of Si-O-M^{+}.[22,23] However, these bands were not observed in the parent NH_4-ZSM-5 sample. In fact, when transition metals such as Mo or V are introduced into the framework of the zeolites by hydrothermal synthesis, an IR band at around 960-970 cm^{-1} can be observed, indicating that the appearance of this IR band is associated with incorporation of the heteroatom into the framework.[24,25] According to previous data for highly dispersed MoO_3 and V_2O_5, a vibrational band either due to Mo=O or V=O groups can be observed at around 900-1000 cm^{-1}.[26,27]

3.5 ^{27}Al MAS-NMR

^{27}Al MAS NMR spectra of both zeolite catalysts and support are presented in Fig. 3. The spectra of the NH_4-ZSM-5 support shows a strong signal centered at 54 ppm corresponding to the different tetrahedral framework Al species[28] and a peak centered at 0 ppm corresponding to the octahedrally coordinated extra-framework Al species.[29] Incorporating V and Mo ions in the exchange sites of zeolite caused a slightly decrease in the peak intensity of the framework Al, while its half-height line width broadens, however the intensity of octahedral Al peak were sharply increased. For the Mo/ZSM-5 sample, a new peak at about -13 ppm appears and this peak can be attributed to the octahedral aluminum in $Al_2(MoO_4)_3$ phase.[30,31] Moreover, a new peak at 14 ppm can be clearly resolved in the ^{27}Al MAS NMR spectra of Mo/ZSM-5 sample. This peak can be due to the hydrated form of an $Al_2(MoO_4)_3$ phase with a tentative formula of $[Al(OH)_n(H_2O)_{6-n}]_n(MoO_4)$ (n = 1 or 2).[30,32] Furthermore, another peak appeared at 38 ppm may be assigned to penta-coordinated non-framework aluminum.[33] It seems that the interaction between Mo species and the ZSM-5 support is so strong that aluminum is extracted by Mo species from the zeolitic framework, and finally leads to the formation of $Al_2(MoO_4)_3$ phase. On the other hand, this new aluminum molybdates phase was not detected by XRD on the Mo/ZSM-5 catalyst. We suggest that, $Al_2(MoO_4)_3$ may be formed in amorphous phase or small $Al_2(MoO_4)_3$ crystallites are present in either at nano-crystalline state (< 4 nm in diameter) that cannot be detected from XRD. On the other side, only little change could be detected on the NMR spectra of V-Mo/ZSM-5.

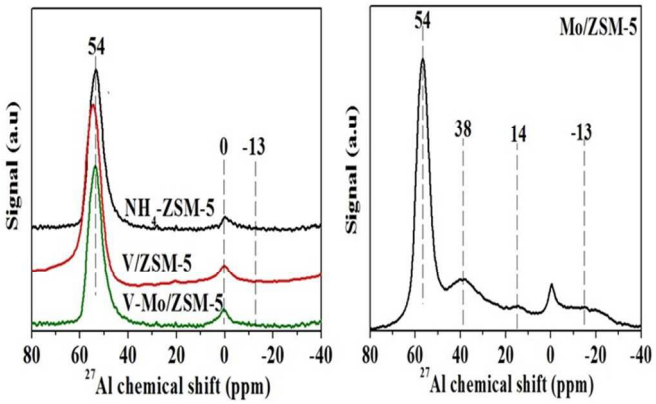

Fig. 3 ^{27}Al MAS-NMR spectra of the support and catalysts.

This means that the original framework of NH_4-ZSM-5 zeolite in V-Mo/ZSM-5 is remained if Mo loading is as low as 2 wt.% and the interaction between Mo species and NH_4-ZSM-5 is not so strong. With increasing Mo loading (6 wt.% in Mo/ZSM-5 catalyst), the interaction between Mo species and NH_4-ZSM-5 zeolite intensifies

which in turn leads to dealumination of the framework of the parent zeolite. Li et al.[34] reported that, at higher Mo loadings, the interaction between Mo species and H-Beta support is so strong that it results in an extraction of aluminum from the zeolite framework, and subsequently appearance of crystalline $Al_2(MoO_4)_3$ phase. This may suggest that the addition of vanadium to monometallic sample affect the interaction between Mo species and NH_4-ZSM-5 zeolite and then the distribution of different Mo species.

3.6 ^{29}Si MAS-NMR

The ^{29}Si MAS NMR spectra of the investigated samples are shown in Fig. 4. The deconvoluted ^{29}Si MAS NMR spectra present five bands at about -103, -107, -110, -111 and -114 ppm. These bands are classically obtained on ZSM-5 zeolites[31,35] and are attributed to tetrahedral Si atoms in $Si(OSi)_{4-n}(OAl)_n$ environment $0 \le n \le 4$. For ZSM-5 zeolite, only Si(0Al) and Si(lA1) configurations exist because its SiO_2/Al_2O_3 ratio is larger than 12.[36,37] The resonances between -103 and -108 ppm correspond to Si(1Al) sites one neighboring and the bands above -110 ppm were assigned to Si(0Al) sites.[38] Table 3 lists the results in more detail. The spectra of all investigated samples do not show the bands with chemical shifts below -100 ppm representing Si(2Al) sites with two Al neighbors. This gives clear evidence that Al–O–Si–O–Al sequences are absent in our samples. The framework Si/Al_{FR}ratio can be calculated according to the equation given by Klinowski[39]:

$$Si/Al_{FR} = \frac{\sum_{n=0}^{4} I Si(nAl)}{\sum_{n=0}^{4} \left(\frac{1}{4}\right) n I Si(nAl)},$$

$I_{Si(nAl)}$: relative areas (%) of Si(nAl) bands attributed to the silicon atoms surrounded by n aluminium atoms (with $0 \le n \le 4$).

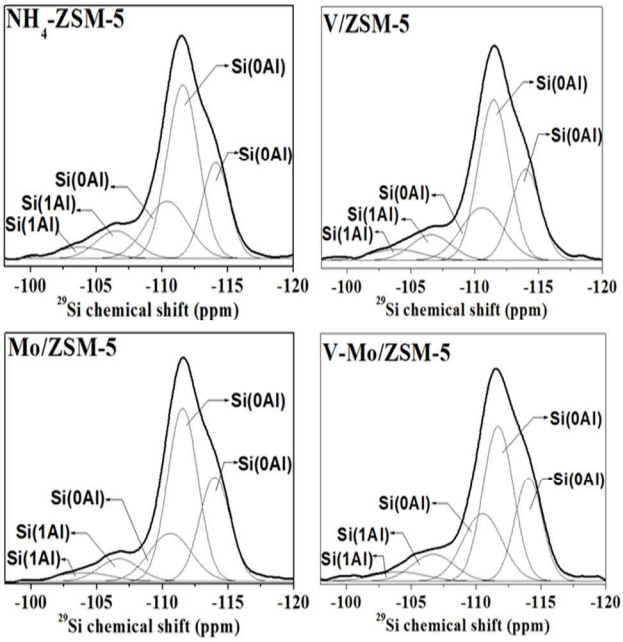

Fig.4 Experimental (bold lines) and deconvoluted (weak lines) ^{29}Si MAS NMR spectra of the support and catalysts.

For the samples NH_4-ZSM-5, V/ZSM-5 and V-Mo/ZSM-5, the Si/Al_{FR} ratios calculated from the spectra are 28.9, 28.9 and 29.4, respectively. These values of Si/Al_{FR} correspond well to the Si/Al values obtained from the chemical analysis. It can be seen that the dealumination is negligible in these samples. Except for Mo/ZSM-5 sample, the Si/Al_{FR} increases sharply. This is consistent with the results from ^{27}Al MAS NMR experiments that the amount of framework Al decreases in the case of Mo/ZSM-5 sample. The above results show that Mo species interact with the framework aluminum of NH_4-ZSM-5 zeolite, and the interaction becomes stronger in the case of Mo/ZSM-5 sample which leads to a low extraction of framework aluminum and the formation of the $Al_2(MoO_3)_4$ nanocrystallites on this catalyst.

Table 3 The deconvolution results of ^{29}Si MAS NMR spectra.

Sample	Si(nAl) site	^{29}Si shift (ppm)	Area (rel. %)	Si/Al_{FR}
NH_4-ZSM-5	Si(1Al)	-103.8	4.8	
		-106.5	9	
	Si(0Al)	-110.4	19.7	28.9
		-111.6	45.3	
		-114.1	21.2	
V/ZSM-5	Si(1Al)	-103.9	4.9	
		-106.6	8.9	
	Si(0Al)	-110.6	19.4	28.9
		-111.5	43.4	
		-114	23.4	
Mo/ZSM-5	Si(1Al)	-104	4	
		-106.7	7.5	
	Si(0Al)	-110.6	17	34.7
		-111.5	44.5	
		-114	27	
V-Mo/ZSM-5	Si(1Al)	-103.8	4.1	
		-106.5	9.5	
	Si(0Al)	-110.4	22.3	29.4
		-111.7	40.1	
		-114.1	24	

3.7 UV–vis spectroscopy

Fig. 5a-b depicts the UV/VIS-DRS spectra of Mo/ZSM-5 and V-Mo/ZSM-5 samples. The UV/VIS-DRS spectrum of Mo/ZSM-5 can be deconvoluted into 3 Gaussian lines which are assigned to Mo^{6+} ions surrounded by oxygen anions in tetrahedral monomeric species (215 nm) and to the dimer or polymerized molybdate species (270 nm)[40,41] as well as to MoO_3 crystallites (325 nm).[42] The UV/VIS-DRS spectrum of V-Mo/ZSM-5 can be deconvoluted into 6 Gaussian lines which are assigned to tetrahedral or distorted tetrahedral monomeric (240 and 310 nm) V^{5+} species[43] as well as tetrahedral monomeric Mo^{6+} species (215 nm), oligomeric molybdate species (270 nm) and MoO_3 crystallites (325 nm). The presence of a band near 400–500 nm suggests that this sample contain a low amount of square pyramidal or distorted octahedral V^{5+} species.[44,45] Since our UV/VIS-DRS spectra were recorded under ambient conditions in the presence of water vapor, it is conceivable that a part of pseudo tetrahedral $V{=}O(OS{\equiv})_3$ species (S

can be Si or Al) at the surface of zeolite are converted to pseudo-octahedral $V=O(H_2O)_2(OS\equiv)_3$ species by coordination of water molecules as previously demonstrated for VO_x species on silica by means of in situ UV-Vis Spectroscopy .[43]

The XRD patterns of all catalysts do not show peaks corresponding to crystalline MoO_3. These results suggested that the M-O_x (M = V or Mo) species with different coordination states and local symmetries are present as highly dispersed on the surface of zeolite. Furthermore, it can be seen that all the spectra do not show the d–d band expected in the range 500–800 nm for V^{4+}or Mo^{5+} ions.

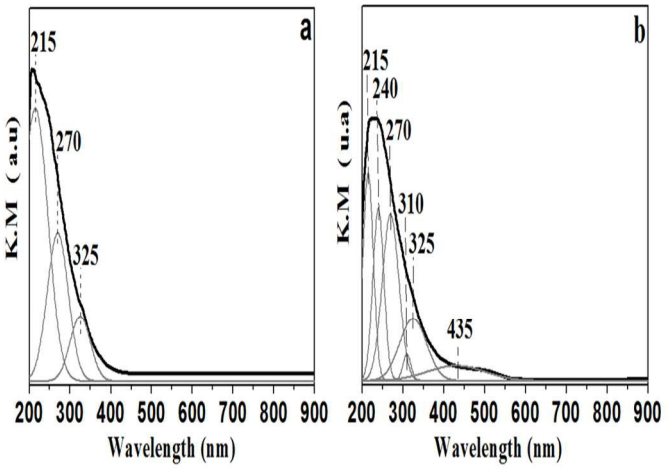

Fig.5 Experimental (bold lines) and deconvoluted (weak lines) UV/VIS-DRS spectra of: (a) Mo/ZSM-5 and (b) V-Mo/ZSM-5.

3.8 Acidity measurements by pyridine adsorption (FT-IR)

The nature of acid sites in calcined samples is characterized by the adsorption of pyridine as a probe molecule and desorption of pyridine at 200 °C. This technique provides useful information on the distinction of Brønsted sites from Lewis sites. IR spectra of pyridine adsorbed on pure ZSM-5 and on the catalysts are shown in Fig. 6. In the spectrum of the parent ZSM-5, the chemisorbed pyridine is identified by the usual set of bands: two bands at 1452 and 1622 cm^{-1} related to Lewis bonded pyridine (L-Py), two bands at 1545 and 1637 cm^{-1} assigned to pyridinium cations (PyH^+) (i.e. Brønsted acid sites) and the superposition of signals of Lewis and Bronsted adsorbed species at 1491 cm^{-1}. It is obvious from the figure that all the samples contain both Brønsted and Lewis acid sites in varying proportions. Pure ZSM-5 solid consists of mainly Brønsted sites with negligible amount of Lewis sites. However, incorporation of V and/or Mo onto ZSM-5 caused a considerable increase in Lewis acidity. This is clearly evidenced from the decrease of the intensity of the band at 1545 cm^{-1} and an increase in the intensity of the band at 1452 cm^{-1}. This finding further confirms the consumption of zeolite protons during the exchange process and the generation of new Lewis acid sites induced by the presence of M-O_x species in the channels of the zeolite. The comparison of the ratio Brønsted sites/Lewis sites (Table 4) also shows that Brønsted acid sites are substituted by Lewis acid ones. Obviously, the Mo species had strong interactions with the Brønsted acid sites of the ZSM-5 and replaced a main part of H^+ sites. The M-O_x species may act as Lewis acid sites as the coordination of vanadium and molybdenum atoms in the small particles or Mo and V species was unsaturated.

Table 4 Catalysts studied by Infrared of chemisorbed pyridine.

Catalyst	Band (19b) Brønsted (cm^{-1})	Band (19b) Lewis (cm^{-1})	I_B/I_L
NH_4-ZSM-5	1545	1456	9.23
V/ZSM-5	1544	1452	5.21
Mo/ZSM-5	1544	1454	2.71
V-Mo/ZSM-5	1544	1454	2.47

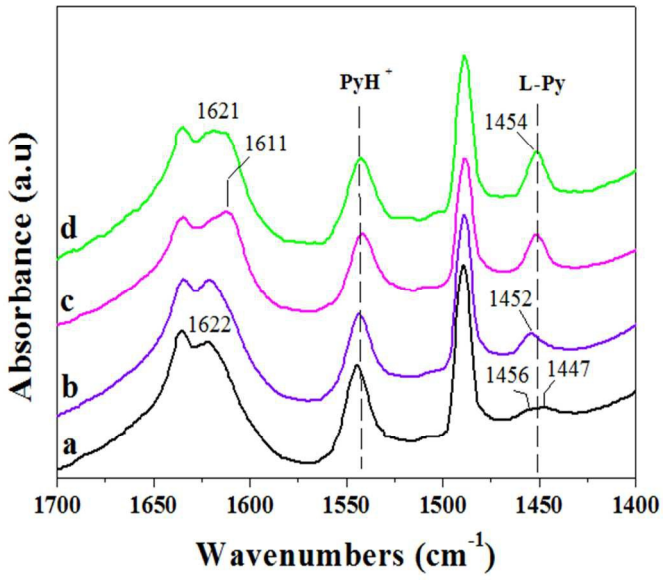

Fig. 6 FTIR spectra of pyridine adsorbed on: (a) NH_4-ZSM-5, (b) V/ZSM-5, (c) Mo/ZSM-5 and (d) V-Mo/ZSM-5.

3.9 XPS spectra

XPS was used to provide information about the oxidation state and the chemical environment of the elements present in the near-surface region of the catalysts. The specific binding energies of the Mo $3d_{5/2}$ and V $2p_{3/2}$ XPS peaks and elemental composition of surface are given in Table 5. The binding energies in the XPS spectra were corrected by referencing to the C 1s 284.80 eV.

For Mo/ZSM-5 sample, the BE of Mo $3d_{5/2}$ component corresponded well with characteristic Mo^{6+} according to literature.[46] Furthermore, in the case of V-Mo/ZSM-5 sample (Fig. 7), the BE of Mo 3d are lower than those of Mo/ZSM-5 as clearly shown in Table 5. This finding indicates that the chemical nature of M-O_x species on the surface of V-Mo/ZSM-5 catalyst differs from those of Mo/ZSM-5 catalyst. The oxidation state of vanadium was determined by the $2p_{3/2}$ (and $2p_{1/2}$) transitions; however, for the latter the O1s satellite signal partially overlapping, then we will discuss only the $V2p_{3/2}$ data here. In the O1s spectra of V/ZSM-5 and V-Mo/ZSM-5 catalysts, a symmetric band was found at around 532.5 eV characteristic of the zeolitic oxygen being structure constituents of the zeolite crystal. Besides the binding energy at 532.5 eV characteristic of zeolitic oxygen, another new signal appeared at 530.5 eV, which is attributed to the oxygen in M-O_x oxides. For the Mo/ZSM-5 sample, a symmetric band was found at around 535.5 eV characteristic of the zeolitic oxygen and a second signal was found at 533.8eV.

Table 5 XPS data for zeolites after ion exchange with vanadium and molybdenum.

Catalyst	Binding energy (eV)		Δ (e V)	Atomic surface concentration (%)				Surface atomic ratio			
	$Mo3d_{5/2}$	$V2p_{3/2}$	$O1s-V2p_{3/2}$	Si 2p	Al 2p	Mo 3d	V 2p	Si/Al	V/Al	Mo/Al	V+Mo/Al
V/ZSM-5	-	516.09	14.5	31.4	1.7	-	0.41	18.5	0.2	-	-
Mo/ZSM-5	233.23	-	-	32.6	1.5	1.8	-	25.8	-	1.2	-
V-Mo/ZSM-5	231.79	516.05	14.4	31.9	1.4	0.3	0.03	22.8	0.02	0.2	0.22

Δ represents the difference in BE between the O1s and V $2p_{3/2}$ line.

From this, it follows that the O1s binding energy obtained from the XPS spectra of different M-O_x oxides are indistinguishable. For V/ZSM-5 and V-Mo/ZSM-5 samples, the $V2p_{3/2}$ signal appears at around 516.1 eV lower than that of V_2O_5 (517.4 eV) reported in the literature.[47] Coulston et al.[48], developed a method for determining an (effective) ''average oxidation state'' V_{eff} in vanadium-based catalysts from the splitting between the O1s and V2p centroids. In the present study, the average vanadium valence state was calculated using the linear relation reported for VO_x sample $V_{eff} = 13.82 – 0.68 [E_b (O1s) – E_b (V2p_{3/2})]$, which gives a value of $V_{eff} \approx 4$ for V/ZSM-5 and V-Mo/ZSM-5 catalysts. However, the UV/VIS-DRS spectra show only absorption bands correspond to ion with d^0 electronic configuration and the samples were subjected to calcination treatments that should oxidize clustered ions to the highest oxidation state. A lot of effort has been made to study the stability of different VO_x samples under the UHV conditions of X-ray photoelectron spectroscopy. For example, the vanadium oxidation state in VPO and alumina-supported VO_x catalysts has been investigated as a function of the time of exposure against vacuum.[48,49] For VPO catalysts, a significant decreasing of V^{+5}/V^{+4} ratio could be observed as a function of the time of exposure to vacuum and a prolonged exposure of the samples to vacuum leads to the appearance of a low-energy components attributed to vanadium in oxidation state of +3 and +2. Similar results were also reported for titania-supported VO_x catalysts, where a remarkably faster reduction of the VO_x was observed. Whereas, a much less pronounced reduction was found for alumina-supported VO_x catalysts. These results suggest that the type of support applied may play an important role in the stability of catalysts under the UHV conditions. In addition, a surface reduction under XPS vacuum can be enhanced by the X-ray radiation. It was reported in the literature that the colors of the solids MoO_3/MCM-41 change after recording the XPS spectra, indicating that the Mo oxide species in the treated samples show the effect of photoinduced reduction. This effect has also been shown for oxides like Nb_2O_5, TiO_2 and V_2O_5 for example, where the preferential sputtering of the oxygen atoms causes a surface reduction.[50] Therefore, one can suggest that the interaction of the X-rays with the zeolite surface during the XPS measurement and the UHV conditions cause a significant reduction of V and Mo species, which are initially present in the highest oxidation state. This finding indicates that conventional X-ray photoelectron spectroscopy under ultra-high vacuum conditions may not necessarily reflect the original oxidation states of the active material.

The V/Al, Mo/Al, and V+Mo/Al atom ratios of bulk composition determined by chemical analysis and of XPS results are shown in Fig. 8. In the case of V/ZSM-5, it is found that the V/Al atom ratios of bulk composition are much larger than that of XPS results, which indicates that a significant part of vanadium may incorporate into the ZSM-5 zeolitic structure.

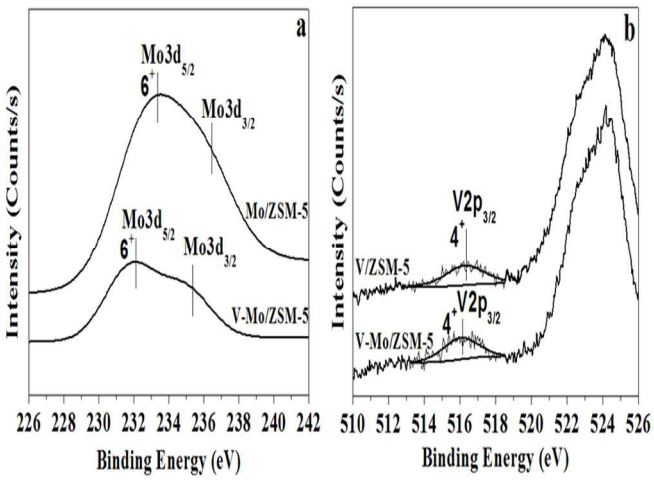

Fig.7 XPS spectra of the catalysts: (a) Mo 3d region; (b) V 2p region.

This is in line with several literature reports proving the movement of vanadium from extra-framework to framework position upon heat treatment at high temperatures.[51] On the other hand, for the V-Mo/ZSM-5 sample, the V/Al and Mo/Al atomic ratios of bulk composition are also larger than those of XPS results. This is in line with FT-IR of pyridine which confirm the consumption of zeolite protons during the exchange process and the generation of new Lewis acid sites induced by the presence of V and Mo ions in the exchange sites inside the pores. It is interesting to note that V/ZSM-5 and V-Mo/ZSM-5 catalysts have the same vanadium content (2wt.%), whereas the V-Mo/ZSM-5 catalyst showed much lower V/Al surface ratio compared to V/ZSM-5. This observation indicates the presence of strong interaction between the V and Mo species in the case of bimetallic sample, which induce a high dispersion of oxide species inside the pores of zeolite. However for Mo/ZSM-5 catalyst, the Mo/Al atomic ratio obtained by XPS is equal to the bulk values indicating the presence of significant amount of molybdenum in the external surface region. Based on the ^{27}Al and ^{29}Si MAS-NMR results that revealed the presence of $Al_2(MoO_4)_3$ phase only in the case of Mo/ZSM-5 sample, we suggest that the increased value of this surface ratio is ascribed to the formation of $Al_2(MoO_4)_3$ nano-crystallites.

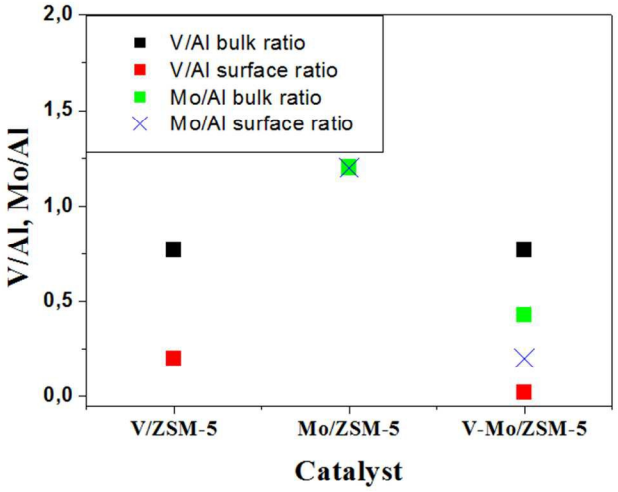

Fig. 8 Surface vs bulk atomic ratios for different catalysts.

3.10 H_2-TPR-O_2-TPO redox cycles

It is known that the redox cycles consisting of temperature programmed reduction (TPR) and reoxidation (TPO) are effective methods to study the redox character of the vanadium and molybdenum centers and the reversibility of the redox behavior of these centers after passing through several redox cycles. In this work, the sequence of TPR–TPO–TPR was studied. Table 6 summarizes The temperatures of the maxima (T_{max}) of the reduction peaks and the H_2/V, H_2/Mo and H_2/V+Mo molar ratios for V/ZSM-5, Mo/ZSM-5 and V-Mo/ZSM-5 catalysts, respectively, in the two successive TPR analyses (1st TPR and 2nd TPR).

The V/ZSM-5 catalyst (Fig. 9a) exhibits three peaks with maxima located at 529, 653 and 726 °C. This is in a range comparable to the data reported in literature.[52-54] However, due to the fact that the profiles obtained in TPR are rather sensitive to the experimental parameters as hydrogen concentration in the gas mixture, heating rate, total flow rate, contact time and sample weight, the number of peaks differs in the publications. The first vanadate reduction peak at 529°C is barely visible; in contrast, the peaks at 653 and 726 °C are significantly more pronounced due to a much higher hydrogen consumption extent. The different peaks are assigned to the reduction of V^{5+} species to V^{3+} species in monomeric or low-oligomeric VO_x surface species and amorphous "bulk-like" V_2O_5.[55] Whereas, the reduction of V^{3+} species to lower oxidation states is unlikely due to the high stability of V_2O_3 even at elevated temperatures.[56] Several TPR investigations of VO_x/SiO_2[57,58] and VO_x/TiO_2[59,60] show that the V_2O_5 -containing catalysts are more difficult to reduce than the vanadate-containing samples, parallel to the decreased degree of V dispersion. Nonetheless, this trend cannot be extended to vanadia on other supports because of the change in the vanadia–support interaction dependent on the electronegativity of the support cation.[61] In fact; Stobbe-Kreemers et al.[62] found that the reduction of monomeric vanadia species on alumina is more difficult than reduction of the polymeric species on this support. Thus, the nature of the support affects the reducibility of the vanadia species. The profile of the Mo/ZSM-5 catalyst (Fig. 9a) shows two broad peaks with maxima located at around 565 and 658 °C. The broadness of the TPR signals indicative of the existence of different molybdate species. In agreement with TPR investigations of Mo/ZSM-5 catalysts,[63,64] the first peak can be assigned to the reduction of two kinds of Mo^{6+} species to Mo^{4+}. The first kind located on the external surface of the zeolite and hence reducible more readily, whereas the second kind associated with Brønsted acid sites in the zeolite that is difficult to reduce. This is in line with the XRD and ^{27}A1 MAS NMR results which show, in the case of Mo/ZSM-5 catalyst, that a part of molybdenum present as MoO_3 and $Al_2(MoO_4)_3$ nano-crystallites dispersed on the external surface of zeolite. At the end of TPR profile, the peak appears with a maximum at 658°C is usually attributed to the reduction of Mo^{4+} to metallic Mo^0.[65, 66] Nevertheless, three well separated peaks at 520, 665 and 769 °C are shown in the TPR profile (Fig. 9a) of the bimetallic V-Mo/ZSM-5 catalyst. An important observation is that T_{max} for the reduction of the bimetallic V-Mo/ZSM-5 catalyst shifts to higher temperatures suggesting that the surface species in the case of bimetallic sample are more difficult to reduce than those in the monometallic ones. Indeed, TPR studies of Mo/ZSM-5 catalyst[67] show that a considerable dispersion of the Mo species gives rise to a significant decrease in the reducibility in comparison with MoO_3. Therefore, the observed shifts toward higher temperatures are indications of increasing dispersion of M-O_x species in V-Mo/ZSM-5 sample. The identification of the TPR peaks for V-Mo/ZSM-5 catalyst is assisted by correlation with the peaks of the monometallic V/ZSM-5 and Mo/ZSM-5 catalysts. Note that the peak at 726 °C for V/ZSM-5 does not appear in the V-Mo/ZSM-5 catalyst. T_{max} at 520 °C is attributed to the reduction of the well-dispersed MoO_3 and V_2O_5 crystallites to MoO_2 and V_2O_3 species respectively, which are located mainly on the external surface of zeolite framework. While T_{max} at 665 °C is assigned to the simultaneous reduction of Mo^{6+} and V^{5+} to Mo^{4+} and V^{3+}, respectively, and the T_{max} at 769 °C is assigned to the reduction of Mo^{4+} to Mo^0. These results indicate a change in the distribution and the nature of M-O_x species in V-Mo/ZSM-5 probably by an interaction between vanadium and molybdenum species such as V-Mo oxo-structure containing V-O-Mo linkages, which are less readily reducible than the M-O_x species. This fact supports the results obtained with other characterization techniques.

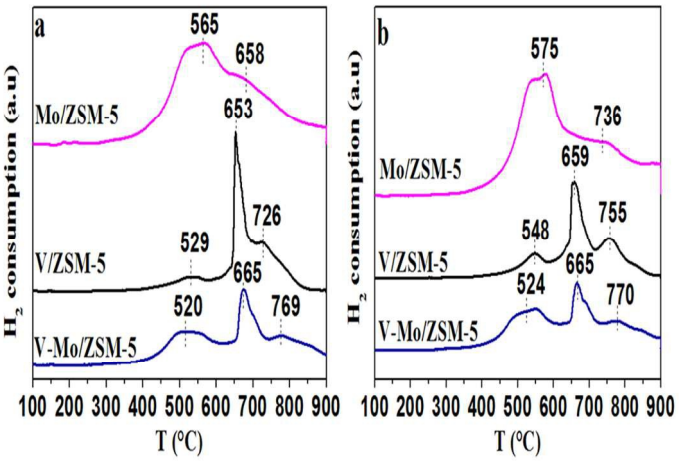

Fig.9 TPR patterns of the catalysts. (a) 1st TPR run patterns of catalysts; (b) 2nd TPR run patterns of catalysts.

The Comparison between the first and second TPR runs (Fig. 9a vs Fig. 9b) reveals several changes in terms of area and position in TPR patterns of the catalysts, except the V-Mo/ZSM-5 sample. For the V/ZSM-5 catalyst, the area of the first reduction peak increases and the third peak becomes more visible, whereas, the area of the second reduction peak remains nearly constant. However, the positions of the first and third peaks originally located at 529 and 726 °C, respectively, shift toward higher temperatures, in contrast,

Table 6 TPR results.

Catalyst	1st TPR in TPR–TPO redox sequences					2nd TPR in TPR–TPO redox sequences				
	T_{1max} (°C)	T_{2max} (°C)	T_{3max} (°C)	H_2 amount (mmol H_2/g)	H_2/M^a	T_{1max} (°C)	T_{2max} (°C)	T_{3max} (°C)	H_2 amount (mmol H_2/g)	H_2/M^a
V/ZSM-5	529	653	726	0.42	0.98	548	659	755	0.41	0.95
Mo/ZSM-5	565	-	658	1.25	2.05	575	-	736	1.30	2.09
V-Mo/ZSM-5	520	665	769	0.79	2.09	524	665	770	0.77	2.03

[a]M = V, Mo or V+Mo

the second peak remains at nearly the same position. The structural changes during H_2/O_2 redox cycles for the vanadia-supported catalyst are in good agreement with the literature[68] which reports that H_2/O_2 redox cycles strengthen the interaction between V species and the support. For the Mo/ZSM-5 catalyst, the area of the first peak increases while the second one decreases. The positions of the two peaks shift toward higher temperatures.

In agreement with the literature,[69] it is evident that the H_2/O_2 redox cycles cause changes in the nature of the surface species in V/ZSM-5 and Mo/ZSM-5 samples. In contrast, the V-Mo/ZSM-5 catalyst shows no significant changes in the corresponding TPR patterns suggesting the good reversibility of the redox behavior of the M-O_x centers in the V-Mo/ZSM-5 sample. Consequently, the bimetallic catalyst presented a more reversible behavior of the M-O_x centers throughout the redox cycle than those in the monometallic ones. The quantitative results of the TPR analyses indicated in Table 6, confirm these conclusions. The full reversibility of the redox cycles in the case of V-Mo/ZSM-5 catalyst indicates the high stability of M-O_x species in the exchange sites of zeolite resulted from the interaction between the V and Mo species.

Based on stoichiometry, H_2/M ratios of either 1 or 3 may be expected, corresponding to reduction of V^{5+} to V^{3+} or Mo^{6+} to Mo^0, respectively. For the V/ZSM-5 catalyst the measured H_2/V ratio is very similar to the expected (stoichiometric) consumption of H_2, indicating that hydrogen completely reduces all vanadia species to the oxidation state +3. Thus, it can be concluded that the dispersed vanadate species in vanadia catalyst are mainly in the initial oxidation state +5. On the other hand, the observed H_2/Mo and H_2/V+Mo ratios for Mo/ZSM-5 and V-Mo/ZSM-5 catalysts, respectively, are smaller than expected (stoichiometric) consumption of H_2. As a rule, the deficit of the hydrogen consumption can be explained by many reasons, namely the presence of non-reducible Mo and/or V species, the presence of a portion of V and/or Mo species in lower oxidation states (V^{4+}, V^{3+} Mo^{5+}, Mo^{4+}…) and an incomplete reduction of V and/or Mo species. In our TPR study, it is obvious that the amount of hydrogen consumption corresponding to the TPR peak at the highest temperature, which is assigned to reduction of Mo^{4+} to metallic Mo^0, was about ½ of that corresponding to the first reduction step, indicating that most Mo^{4+} species could not be thoroughly reduced to metallic Mo^0. This incomplete reduction of Mo^{4+} species to Mo^0 was also reported by other authors for Mo/ZSM-5 catalysts.[65] From these data, it can be concluded that the dispersed V and Mo species in our catalysts are mainly in the highest oxidation states. Nevertheless, the presence of a minor fraction of Mo^{5+} or V^{4+}, which are rather stable even under oxidizing conditions, cannot be totally excluded. Obviously, in the present study, the XPS results may not reflect the original oxidation state of the catalysts but rather that of samples, which are significantly reduced under the experimental vacuum conditions. In fact, the XPS gives information about the surface behavior of the catalyst, that is sensitive only to a few upper layers of the catalyst surface and a reduction under UHV conditions is accompanied by a release of the outer most lattice oxygen species, whereas, the TPR investigates the bulk system, that measures the complete amount of accessible reducible species including deeper layers.

3.11. Catalysis

Ammoxidation reaction of ethylene was carried out in in a temperature window of 425–500 °C. The effect of the reaction temperature on the conversion of ethylene (X-C_2H_4), yield of acetonitrile (Y-ACN) and selectivity to acetonitrile (S-ACN) of various catalysts is displayed in Fig. 10a-c. As expected, the activity of the samples increased with increasing the temperature from 425 °C to 500 °C. ACN is the major product, while CO_2 is the main by-product. At low temperatures, the total oxidation of ethylene to CO_2 is considerably high, which in turn reduces the selectivity of the desired product, ACN. For the most active catalyst (i.e. V-Mo/ZSM-5), the conversion of ethylene and the selectivity toward acetonitrile were observed to increase continually from 3 to 15% and from 65 to 97% across the temperature range, respectively. Therefore, the temperature has a highly pronounced promotional effect on the ammoxidation of ethylene into acetonitrile. The enhancement in the catalytic properties might be attributed to the increase in the intrinsic activity of the existing active sites and also to the creation of more active sites with rise in reaction temperature.

It is clear from the fig. 10a-c that V/ZSM-5 catalyst has much lower activity in ammoxidation of ethylene compared to Mo/ZSM-5 catalyst. At 425 °C, Mo/ZSM-5 catalyst exhibited very low catalytic activity (Y-ACN of 1%) while, V/ZSM-5 catalyst is almost inactive. However, at 500°C, Mo/ZSM-5 catalyst yielded higher C_2H_4 conversion and acetonitrile yields when compared to V/ZSM-5 solid.

According to these results, vanadium was able to catalyze the ammoxidation of ethylene into acetonitrile, but with less efficiency. Nonetheless, molybdenum exhibits reasonably good performance. On the other hand, the bimetallic V-Mo/ZSM-5 catalyst was found to be more active and selective toward acetonitrile than the monometallic Mo/ZSM-5 and V/ZSM-5 catalysts. The order of activity is observed to change in the following manner:

V-Mo/ZSM-5 > Mo/ZSM-5 >> V/ZSM-5

From these results, it is very clear that substituting molybdenum with vanadium has a positive effect both on the activity and the selectivity. This implies clearly that a certain kind of synergetic effect between V and Mo species exists and plays an important role in the ammoxidation reaction.

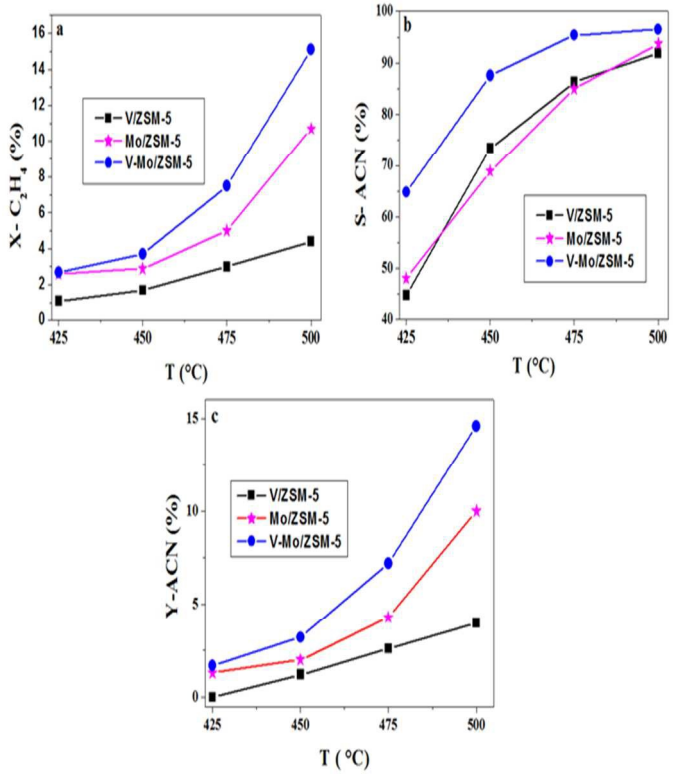

Fig.10 Variation of the catalytic performance (a**:** X-C_2H_4, b: S-ACN and c: Y-ACN) of catalysts with the reaction temperature.

It is well known that ammoxidation of ethylene on the catalyst takes place through a redox mechanism. Li and Armor[3] proposed a mechanism for the ammoxidation of ethylene over Co/ZSM-5 catalyst using a specially designed Temperature Programmed Reaction (TPRx) experiment (reaction between an adsorbed NH_3 and gaseous $C_2H_4/O_2/He$). These authors reported that under the ammoxidation reaction conditions, the addition of gaseous C_2H_4 to the adsorbed NH_3 forming an adsorbed ethylamine molecule, which is then dehydrogenated and forming ethylamine anion ($C_5H_5NH_2$) which is considered as a reaction intermediate. This intermediate is subsequently oxidized by the gaseous O_2 forming the desired product, ACN. Furthermore, Co ions in exchange position as isolated species are considered the active sites in the ammoxidation reaction whereas, polycrystalline cobalt oxide enhance the over oxidation of ethylene to CO_2.[4,] Then, the state and distribution of transition metals species are important for the better performance of catalysts in hydrocarbons ammoxidation.

It is interesting also to point out that metal supported on oxide surfaces were much less active than when exchanged into zeolites (e.g., ZSM-5) as tabulated in Table 7. Cr/Al_2O_3 and Co/Al_2O_3 catalysts were not found to be highly active in ammoxidation of ethylene to acetonitrile, whereas, Cr/ZSM-5 and Co/ZSM-5 catalysts exhibited higher activity (Table 7). This suggests that the support phase is important for the ammoxidation reaction. The enhanced activity for metal exchanged zeolites could be attributed to the enhanced dispersion of the cation sites over the sites within the zeolite which control the coordination, location and distribution of these metal cations. Also, from Table 7 one sees the the different reaction results obtained over a number of metal cations which illustrate the importance of intrinsic activity of a metal cation. As shown in table 7, V-Mo/ZSM-5 is very active and selective catalyst for ethylene ammoxidation.

In our work, all catalysts have been synthesized by solid state ion-exchange method which results in excellent dispersion of metals in ZSM-5. In order to account for the variations in catalytic performance of various catalysts, it is essential to correlate the catalytic activities to V and Mo species distributed on zeolite ZSM-5. For V-Mo/ZSM-5 catalyst, the V and Mo species interacted with the framework of ZSM-5, and decreased the Brønsted acid sites remarkably as clearly shown by the pyridine-IR technique. The structural determination showed that V and Mo species are mainly inside the channel of ZSM-5 probably as monomeric and dimeric species and metal oxides crystallites (less than 4 nm) highly dispersed in the channel and/or on the external surface of zeolite. However, for the Mo/ZSM-5 catalyst the ^{27}Al MAS NMR and ^{29}Si MAS NMR results revealed that a low fraction of aluminum is extracted by Mo species from the zeolitic framework, and finally leads to the formation of $Al_2(MoO_4)_3$ nano-crystallites. These $Al_2(MoO_4)_3$ species are distributed on the external surface of the Mo/ZSM-5 crystals. This result was also supported by the XPS experiment, which indicates the presence of significant amount of molybdenum in the external surface region. Therefore, it is reasonable to consider that substitution of molybdenum with vanadium affects the nature and distribution of Mo species introduced in ZSM-5 zeolite. It is tempting to assume that the activity in ethylene ammoxidation is governed by the isolated Mo species that are located inside the channel of the zeolite; consequently, the Mo/ZSM-5 sample with less of these species manifests lower activity compared to V-Mo/ZSM-5 sample.

Table 7 Comparison between V-Mo/ZSM-5 and other catalytic systems for ethylene ammoxidation[a]

Catalyst	Catalyst weight (g)	X-C_2H_4 (%)	S-ACN (%)	Reference
V-Mo/ZSM-5	0.05	15	97	This work
Mo/ZSM-5	0.05	11	94	This work
Co/ZSM-5	0.05	19	98	[70]
Cr/ZSM-5	0.1	15	93	[5]
Cr/Al_2O_3	0.1	8	83	[71]
Co/Al_2O_3	0.1	10	85	[71]

[a]All catalysts were tested tat 500 °C, feed consisted of 10% C_2H_4 ; 10% NH_3 ; 10% O_2 in He with a total flow rate of 100 cm^3/min.

A second observation is that the V-Mo/ZSM-5 catalyst exhibited a more reversible behavior of the M-O_x centers throughout the H_2/O_2 redox cycles than those in V/ZSM-5 and Mo/ZSM-5 catalysts. As mentioned previously, the catalytic ammoxidation of ethylene is assumed to be based on reduction–reoxidation cycles. Nevertheless, under reaction conditions or redox cycles, the Tammann temperature is exceeded significantly, thus surface mobility of V and Mo species becomes likely which can even cause changes in the nature of the surface species.[72] TPR and TPO studies revealed the full reversibility of the redox cycles in the case of V-Mo/ZSM-5 catalyst, which is related to the high stability of M-O_x species in the exchange sites of zeolite. It is reasonable to consider that the V species interacted with Mo ions in the exchange sites and then increase the stability of Mo species in the inside the channel of

the zeolite due to their lack of mobility. Accordingly, the better catalytic performance of V-Mo/ZSM-5 catalyst is more likely due to the presence of V^{5+}-O-Mo^{6+} bonds.

From our results, it became obvious that the observed synergism in the ammoxidation reaction for the V-Mo/ZSM-5 catalyst is related to the existence of electronic interaction at short range order between the V and Mo species, which may influence the catalyst redox properties. In fact, VO_x species are supposed to modify the redox potential of the main redox couple (Mo^{6+} /Mo^{5+}) via a co-redox system (V^{5+}/V^{4+} with Mo^{6+} /Mo^{5+}).

A synergetic effect between Mo and V is not so surprising. Banãres and co-workers[14] studied a Mo–V-mixed oxides supported on Al_2O_3 in the ODH of propane and reported an enhanced reaction rate and a higher propylene formation when vanadium oxide was supported on Al_2O_3 containing a nominal polymolybdate layer. They proposed that the better catalytic performance of mixed Mo–V-catalysts was ascribed to the formation of mixed Mo–V–O species.

On the other hand, the addition of vanadium can change the space structure between active sites which leads to lower concentrations of Mo^{6+}-O-Mo^{6+} bonds. According to the literature, when the active sites are juxtaposed, the desorption of intermediate reactant molecules ($C_5H_5NH_2$) could be discouraged, in contrast, when the active sites are spatially too separated, the interaction of ethylamine molecules decreases and thereby facilitates their desorption. Hence, a possible explanation for the higher activity and selectivity to acetonitrile obtained in the case of bimetallic sample compared to the monometallic ones is that V species isolate the catalytically active centers (site isolation) from each other. This situation facilitates the ethylamine molecules desorption and prevents the unwanted over-oxidation to CO_2.

Conclusions

In the present study, vanadium, molybdenum and Vanadium-molybdenum supported on zeolite ZSM-5 catalysts were investigated to evaluate structural properties, redox cycles and the effect of vanadium on the properties of molybdenum. The catalytic properties of the catalysts were evaluated for the ammoxidation of ethylene to acetonitrile. It was found that the substitution of molybdenum with vanadium shown a substantial influence on the physico-chemical characteristics (e.g. nature of MoO_x species, reducibility, surface composition etc.) of catalysts and as well as the catalytic properties. As proved by the pyridine-IR technique, the V and Mo species react with zeolite protons during the exchange process and generate new Lewis acid sites in the channels of the zeolite. The M-O_x species are essentially, monomeric and dimeric/polymeric species or metal oxides crystallites (less than 4 nm), which are highly dispersed in the channel and/or on the external surface of zeolite. Additionally, the ^{27}A1 and ^{29}Si MAS-NMR experiments revealed the formation of $Al_2(MoO_4)_3$ nano-crystallites in the case of Mo/ZSM-5 sample due to the strong interaction between Mo species and the support. This observation was confirmed by the XPS analysis that exhibited the presence of significant amount of molybdenum in the external surface region. The best performance was achieved over the bimetallic V-Mo/ZSM-5 catalyst. These results showed that a synergetic effect between V and Mo species play an important role in the ammoxidation reaction. It seems that the formation of the $Al_2(MoO_4)_3$ causes the catalysts to become less active for ethylene ammoxidation. Structural changes were investigated on exposure of all catalysts to H_2/O_2 redox environment. It was found that the H_2/O_2 redox cycles cause changes in the nature of the surface species in V/ZSM-5 and Mo/ZSM-5 samples. However we note a full reversibility of the redox cycles in the case of V-Mo/ZSM-5 catalyst, suggesting, the high stability of M-O_x species in the exchange sites of zeolite resulted from the interaction between the V and Mo species. Thus the interaction between V and Mo species improve the catalyst redox properties and thereby catalytic activity and selectivity as well.

Acknowledgements

The authors like to thank Prof. Michael Hunger from University of Stuttgart for MAS NMR studies.

References

1 A.H. Tullo, *Chem.Eng.News*, 2009, **87**, 9.

2 S.M. Aliev, V.D. Sokolovskii, G.B. Boreskov; USSR Patent SU 738 657: Chem. Abstract 93:121053y, 1980.

3 Y. Li, J.N. Armor, *J. Catal.*, 1998, **176**, 495–502.

4 M. Mhamdi, S. Khaddar-Zine, A. Ghorbel, *Appl. Catal. A*, 2009, **357**, 42–50.

5 F. Ayari, M. Mhamdi, T. Hammedi, J. Álvarez-Rodríguez, A.R. Guerrero-Ruiz, G. Delahayc, A. Ghorbel, *Appl. Catal. A*, 2012, **439–440**, 88–100.

6 J. Thoret, C. Marchal, C. Dordmieux-Morin, P.P. Man, M. Gruia, J. Fraissard, *Zeolites*, 1993, **13**, 269-275.

7 H.G. Karge, H.K. Beyer, in: P.A. Jacobs (Ed.), Zeolite Chemistry and Catalysis, *Stud. Surf. Sci. Catal.*, 1991, **69**, 43–64.

8 A.V. Kucherov, A.A. Slinkin, *J. Mol. Catal.*, 1994, **90**, 323–354.

9 R. Bulanek, K. Novoveska, B. Wichterlova, *Appl. Catal. A*, 2002, **235**, 181–191.

10 M. Mhamdi, S. Khaddar-Zine, A. Ghorbel, *Stud. Surf. Sci. Catal.*, 2002, **142**, 935–942.

11 H. Liu, X. Bao, Y. Xu, *J. Catal.*, 2006, **239**, 441–450.

12 Y. Shu, M. Ichikawa, *Catal. Today*, 2001, **71**, 55–67.

13 X. Wang, S. Yu, H. Yang, S. Zhang, *Appl. Catal. B*, 2007, **71**, 246-253.

14 M.A. Banãres, S.J. Khatib, *Catal. Today*, 2004, **96**, 251–257.

15 M.O. Guerrero-Perez, J. L. G. Fierro, M. A. Vicente, M. A. Banãres, *J. Catal.*, 2002, **206**, 339–348.

16 A.M. Monti, A. Baiker, *J. Catal.*, 1983, **83**, 323–335.

17 V.M. Bondareva, T.V. Andrushkevich, O.B. Lapina, *Catal. Today*, 2000, **61**,173–178.

18 A. Gervasini, *Appl. Catal. A*, 1999, **180**, 71–82.

19 K.F.M.G.J. Scholle, W. S. Veeman, P. Frenken, G.P.M. Van de Velden, *Appl. Catal.*, 1985, **17**, 233–259.

20 J.C. Jansen, F.J. Van der Gaag, H. Van Bekken, *Zeolites*, 1984, **4**, 369–372.

21 E.M. Flaningen, H. Khatami, H.A. Szymanski, *Adv. Chem. Ser.*, 1971, **101**, 201–229.

22 G. Ramis, G. Busca, V. Lorenzelli, *Z. Phys. Chem., Neue Folge*, 1987, **153**, 189–200.

23 L. Lietti, I. Nova, G. Ramis, L. DallAcqua, G. Busca, E. Giamello, P. Forzatti, F. Bregani, *J. Catal.*, 1999, **187**, 419–435.

24 A. Tuel, Y. B. Taarit, *Zeolites*, 1994, **14**, 18–24.

25 A. Thangaraj, R. Kumar, P. Ratnasamy, *Appl. Catal.*, 1990, **57**, L1–L3.

26 W.G. Klemperer, V.V. Mainz, R.C. Wang, W. Shum, *Inorg. Chem*., 1985, **24**, 1970–1971.

27 M. Anpo, H. Yamashita, In Surface Photochemistry, M. Anpo, (Ed.), Wiley: London, 1996, 117–164.

28 H. Ichihashi, M. Ishida, A. Shiga, M. Kitamura, T. Suzuki, K. Suenobu, K. Sugita , *Catal. Surveys Asia*, 2003, **7**, 261–270.

29 H. Sato, N. Ishii, K. Hirose, S. Nakamura, In: Proceedings of seventh international zeolite conference, 1986, 755.

30 W.P. Zhang, D. Ma, X.W. Han, X.M. Liu, X.H. Bao, X.W. Guo, X.S.Wang, *J. Catal.*, 1999, **188**, 393–402.

31 W. Liu, Y.D. Xu, S.T. Wong, L. Wang, J. Qiu, N. Yang, *J. Mol. Catal.*, 1997, **120**, 257–265.

32 D. Ma, Y.Y. Shu, X.W. Han, X.M. Liu, Y.D. Xu, X.H. Bao, *J. Phys. Chem. B*, 2001, **105**, 1786–1793.

33 F. Deng, Y. Du, C. Ye, J. Wang, T. Ding, H. Li, *J. Phys. Chem.*, 1995, **99**, 15208–15214.

34 X. Li, W. Zhang, S. Liu, X. Han, L. Xu, X. Bao, *J. Mol. Catal.*, 2006, **250**, 94–99.

35 C.A. Fyfe, G.C. Gobbi, G.J. Kennedy, *J. Phys. Chem.*, 1984, **88**, 3248–3253.

36 J. Brothers and J. Pentel, U.S. Patent 3842741, 1974.

37 V.G. Stepanov, A.A. Shubin, K.G. lone, V.M. Mastikhin and K.I. Zamaraev, *Kinet. Katal.*, 1984, **25**, 1225.

38 Y. Chen, L. Dai and Z. Xue, *Acta Chim. Sin.*, 1994, **52**, 716–721.

39 J. Klinowski, S. Ramdas, J.M. Thomas, C.A. Fyfe, J.S. Hartman, *J. Chem. Sot. Faraday Trans. 1*, 1982, **78**, 1025–1050.

40 X. Wang, S. Yu, H. Yang, S. Zhang, *Appl. Catal. B*, 2007, **71**, 246–253.

41 G. Xiong, Z. Feng, J. Li, Q. Yang, P. Ying, Q. Xin, C. Li, *J. Phys. Chem. B*, 2000, **104**, 3581–3588.

42 A. de Lucas, J.L. Valverde, L. Rodriguez, P. Sanchez, M.T. Garcia, *Appl. Catal. A*, 2000, **203**, 81–90.

43 H. Berndt, A. Martin, A. Brückner, E. Schreier, D. Müller,H. Kosslick, G.U. Wolf, B. Lücke, *J. Catal.*, 2000, **191**, 384–400.

44 M. Morey, A. Davidson, H. Eckert, G. Stucky, *Chem. Mater.*, 1996, **8**, 486–492.

45 M. Schraml-Marth, A. Wokaun, M. Pohl, H.Ludwig Krauss, *J. Chem. Soc. Faraday Trans.*, 1991, **87**, 2635–2646.

46 B.M. Reddy, B. Chowdhury, P.G. Smirniotis, *Appl. Catal. A*, 2001, **211**, 19–30.

47 W.E. Slinkard and P.B. Degroot, *J. Catal.*, 1981, **68**, 423–432.

48 G.W. Coulston, E.A. Thompson, N. Herron, *J. Catal.*, 1996, **163**, 122–129.

49 Y. Suchorski, L. Rihko-Struckmann, M. Alandjiyska, K. Sundmacher, F. Klose, H. Weiss,Y.Ye, *Appl. Surf. Sci.*, 2005, **249**, 231–237.

50 G. Betz, G.K. Wehner, in: R. Behrisch (Ed.), Sputtering by Particle Bombardment II, Springer-Verlag, Berlin, 1983,11.

51 A.V. Kucherov, A.A. Slinkin, *J. Mol. Catal.*, 1994, **90**, 323–354.

52 F. Arena, F. Frusteri, A. Parmaliana, *Appl. Catal. A*, 1999, **176**, 189–199.

53 K.V.R. Chary, G. Kishan, C.P. Kumar, G.V. Sagar, *Appl. Catal. A*, 2003, **246**, 335–350.

54 M.M. Koranne, J.G. Goodwin Jr., G. Marcelin, *J. Catal.*, 1994, **148**, 369–377.

55 K. Chen, A.T. Bell, E. Iglesia, *J. Catal.*, 2002, **209**, 35–42.

56 J. Haber, M. Witko, R. Tokarz, *Appl. Catal. A Gen.*, 1999, **157**, 3–22.

57 A. Parmaliana, F. Arena, *J. Catal.*, 1997, **167**, 57–65.

58 F. Arena, N. Giordano, A. Parmaliana, *J. Catal.*, 1997, **167**, 66–76.

59 G. Bond, S.F. Tahir, *Appl. Catal.*, 1991, **71**, 1–31.

59 H.K. Matralis, C. Papadopoulou, C. Kordulis, A.A. Elguezabal, V.C. Corberan, *Appl. Catal. A*, 1995, **126**, 365–380.

61 M. A. Banãres, M. V. Martinez-Huerta, X. Gao, J.L.G. Fierro, I. E. Wachs, *Catal. Today*, 2000, **61**, 295–301.

62 A.W. Stobbe-Kreemers, G.C. van Leerdam, J.P. Jacobs, H.H. Brongersma, J. J. F. Scholten, *J. Catal.*, 1995, **152**, 130–136.

63A. Antiñolo, P. Cañizares, F. Carrillo-Hermosilla, J. Fernández-Baeza, A. de Lucas, A. Otero, L. Rodrıguez , J.L. Valverde, *Appl. Catal. A*, 2000, **193**, 139–146.

64 D. Ma, Y. Shu, X. Bao, Y. Xu, *J. Catal.*, 2000, **189**, 314–325.

65 H. Liu, X. Bao, Y. Xu, *J. Catal.*, 2006, **239**, 441–450.

66 H. Liu , Y. Xu, *Chin. J. Catal.*, 2006, **27**, 319–27.

67 A. Antiñolo, P. Cañizares, F. Carrillo-Hermosilla, J. Fernández-Baeza,A. de Lucas, A. Otero, L.Rodrıguez , J.L. Valverde, *Appl. Catal. A*, 2000, **193**, 139–146.

68 F. Klose, T. Wolff, H. Lorenz, A. Seidel-Morgenstern, Y. Suchorski, M. Piórkowska, H. Weiss, *J. Catal.*, 2007, **247**, 176–193.

69 N. Ballarini, F. Cavani, A. Cericola, C. Cortelli, M. Ferrari, F. Tifirò, G. Capannelli, A. Comite, R. Catani, U. Cornaro, *Catal. Today*, 2004, **91–92**, 99–104.

70 M. Mhamdi, S. Khaddar-Zine, A. Ghorbel, *Appl. Catal. A, 2008,* **337**, 39–47.

71 F. Ayari, M. Mhamdi, G. Delahay, A. Ghorbel, *J. Sol–Gel Sci. Technol.*, 2009, **49 (2)**, 170–179.

72 I.E. Wachs, Y. Chen, J.M. Jehng, L.E. Briand, T. Tanaka, *Catal. Today*, 2003, **78**, 13–24.